Received: 2 February 2024 | Revised: 26 April 2024 | Accepted: 10 May 2024

DOI: 10.1002/agt2.600

Aggregate Open Access WILEY

RESEARCH ARTICLE

Spatiotemporal responsive hydrogel microspheres for the treatment of gastric cancer

Li Wang[1,2,3] | **Lu Fan**[2,3] | **Anne M. Filppula**[2] | **Yu Wang**[1,3] | **Luoran Shang**[4] | **Hongbo Zhang**[1,2,5]

[1]Joint Centre of Translational Medicine, Wenzhou Key Laboratory of Interdiscipline and Translational Medicine, The First Affiliated Hospital of Wenzhou Medical University, Wenzhou, China

[2]Pharmaceutical Sciences Laboratory, Åbo Akademi University, Turku, Finland

[3]Oujiang Laboratory (Zhejiang Lab for Regenerative Medicine, Vision and Brain Health), Wenzhou Institute, University of Chinese Academy of Sciences, Wenzhou, Zhejiang, China

[4]Shanghai Xuhui Central Hospital, Zhongshan-Xuhui Hospital, the Shanghai Key Laboratory of Medical Epigenetics, the International Co-laboratory of Medical Epigenetics and Metabolism (Ministry of Science and Technology), Institutes of Biomedical Sciences, Fudan University, Shanghai, China

[5]Turku Bioscience Centre, University of Turku and Åbo Akademi University, Turku, Finland

Correspondence
Hongbo Zhang, Pharmaceutical Sciences Laboratory, Åbo Akademi University, Turku 20520, Finland.
Email: hongbo.zhang@abo.fi

Luoran Shang, Institutes of Biomedical Sciences, Fudan University, Shanghai 200032, China.
Email: luoranshang@fudan.edu.cn

Yu Wang, Wenzhou Institute, University of Chinese Academy of Sciences, Wenzhou, Zhejiang 325001, China.
Email: 1146681561@qq.com

Funding information
National Natural Science Foundation of China, Grant/Award Number: 82372145; Research Fellow, Grant/Award Number: 353146; Research Project, Grant/Award Number: 347897; Solutions for Health Profile, Grant/Award Number: 336355; InFLAMES Flagship, Grant/Award Number: 337531; Finland China Food and Health International Pilot project funded by Finnish MInistry of Education and Culture

Abstract

The development of tumor drug microcarriers has attracted considerable interest due to their distinctive therapeutic performances. Current attempts tend to elaborate on the micro/nano-structure design of the microcarriers to achieve multiple drug delivery and spatiotemporal responsive features. Here, the desired hydrogel microspheres are presented with spatiotemporal responsiveness for the treatment of gastric cancer. The microspheres are generated based on inverse opals, their skeleton is fabricated by biofriendly hyaluronic acid methacrylate (HAMA) and gelatin methacrylate (GelMA), and is then filled with a phase-changing hydrogel composed of fish gelatin and agarose. Besides, the incorporated black phosphorus quantum dots (BPQDs) within the filling hydrogel endow the microspheres with outstanding photothermal responsiveness. Two antitumor drugs, sorafenib (SOR) and doxorubicin (DOX), are loaded in the skeleton and filling hydrogel, respectively. It is found that the drugs show different release profiles upon near-infrared (NIR) irradiation, which exerts distinct performances in a controlled manner. Through both in vitro and in vivo experiments, it is demonstrated that such microspheres can significantly reduce tumor cell viability and enhance the efficiency in treating gastric cancer, indicating a promising stratagem in the field of drug delivery and tumor therapy.

KEYWORDS
combination therapy, gastric cancer, inverse opal, microcarriers, spatiotemporal responsiveness

1 | INTRODUCTION

The increasing incidence of cancer has brought huge burden to the current social medical system.[1–3] Tremendous efforts are devoted to cancer treatment including drug therapy, radiation therapy, and surgical resection.[4–7] Of these, drug therapy remains an effective stratagem.[8,9] For instance, doxorubicin (DOX), a common chemotherapeutic drug, has demonstrated its efficacy against various types of cancers.[10–12] Additionally, target-therapeutic drugs like sorafenib (SOR) are often used as a combinatory agent to overcome the limitations of traditional monochemotherapy.[13–15] Although such synergistic therapy shows great progress,[16,17] systemic and frequent administration of the drugs may lead to severe adverse effects, such as organ toxicity and anaphylaxis.[18,19] To handle these, microcarriers, particularly those based on photothermal materials such as black phosphorus, have garnered considerable attention.[20] Their remarkable photothermal conversion capabilities, coupled with the use of near-infrared irradiation, enable microcarriers to achieve

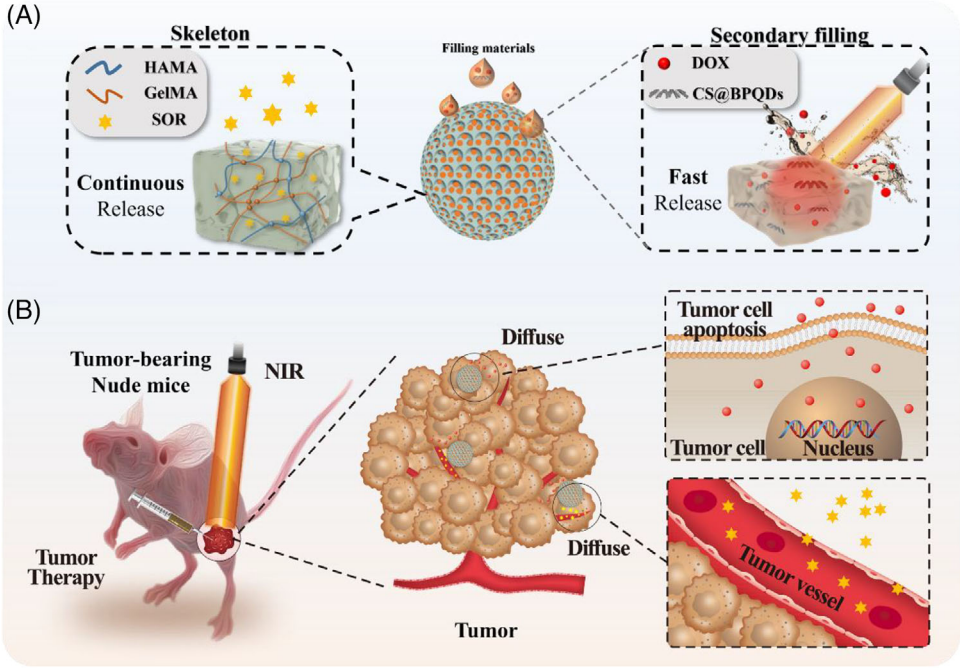

FIGURE 1 Scheme of spatiotemporal responsive hydrogel microspheres and their application for gastric cancer therapy. (A) Scheme of the skeleton and secondary filling network. (B) Spatiotemporal responsive hydrogel microspheres applied in gastric cancer synergistic treatment. The continuous release of SOR inhibited blood vessel growth. The fast release of DOX led to tumor cell apoptosis.

controlled drug release within tissues.[21,22] However, the treatment cycle and duration of different drugs are not the same, and it remains challenging to specifically control the delivery of several drugs in a single system.[23–25] Therefore, a novel combination chemotherapy strategy with spatiotemporal control of the release profile of different drugs is urgently needed to achieve efficient tumor therapy.

Herein, we present an ideal dual drug delivery system based on inverse opal microparticles (IOMPs) with spatiotemporal responsiveness for gastric cancer therapy, as schemed in Figure 1. IOMP is a material characterized by a skeleton and regularly arranged 3D nanovoids.[26–29] The skeleton of IOMPs typically features a connected hydrogel network, while the nanopore spaces can be refilled with a secondary material of different properties from those of the skeleton.[30,31] Based on this, composite IOMPs can be fabricated and serve as microcarriers for delivery of multidrugs.[32,33] Compared to microcarriers with a homogeneous structure and component, the skeleton and filling material of such composite IOMPs offer distinct compartments for accommodating different drugs.[34] Additionally, the release profile of each drug can be modulated by controlling the physicochemical properties of the skeleton and secondary filling material separately. Thus, it is conceivable to develop an innovative drug delivery system based on IOMPs possessing exceptional spatiotemporal responsiveness behaviors and thus achieving two different drug release modes.

Herein, we fabricated the desirable IOMPs-based drug delivery system with SOR loaded in the skeleton and DOX encapsulated in a reversible phase-changing hydrogel, which was further filled into the nanovoids. The IOMPs were obtained by using a photocured hydrogel polymer to replicate a photonic crystal template. The skeleton hydrogel mainly consisted of hyaluronic acid methacrylate (HAMA), gelatin methacrylate (GelMA), and SOR. Then, fish gelatin/agarose, a reversible phase-changing hydrogel, served as the secondary material to fill in the IOMPs nanovoids, with DOX incorporated. Notably, black phosphorus quantum dots (BPQDs) were doped in the secondary filling material too. Attributing to the efficient photothermal conversion ability of BPQDs, the secondary hydrogel achieved a direct gel–sol phase transition via near-infrared irradiation, which promoted the release of DOX at the tumor site. In comparison, SOR was released continuously from the IOMPs skeleton, thus impeding angiogenesis and tumor growth. Utilizing such characteristics, it has been verified that dual drug-loaded composite IOMPs possessed the desired properties of on-demand drugs release and enhanced the therapeutic efficiency of gastric cancer. These results revealed that the spatiotemporal responsive hydrogel microspheres possessed valuable application potential for drug delivery and tumor therapy.

2 | RESULTS AND DISCUSSION

In a typical experiment, the spatiotemporal responsive hydrogel microspheres were fabricated, as illustrated in Figure 2A. Firstly, silica photonic crystals (PhCs) templates were generated by self-assembly of silica nanoparticles using droplet microfluidic technology. The hexagonal stacking of nanoparticles gave the microspheres periodically arranged nanoholes, and the photonic band gap effect caused by this special structure endowed them with bright visible structural color. As shown in Figure 2B, a series of derived microspheres, including hybrid PhCs, inverse opal, and composite microspheres, absolutely inherited this optical property, which was attributed to their ordered structures. To further explore this, scanning electronic microscopy (SEM) was used to characterize the structural feature of these microspheres, and it showed that the PhC template exhibited regular hexagonal packing structures both at the surface and in the interior (Figure 2C-i). For hybrid PhCs, the polymer was completely

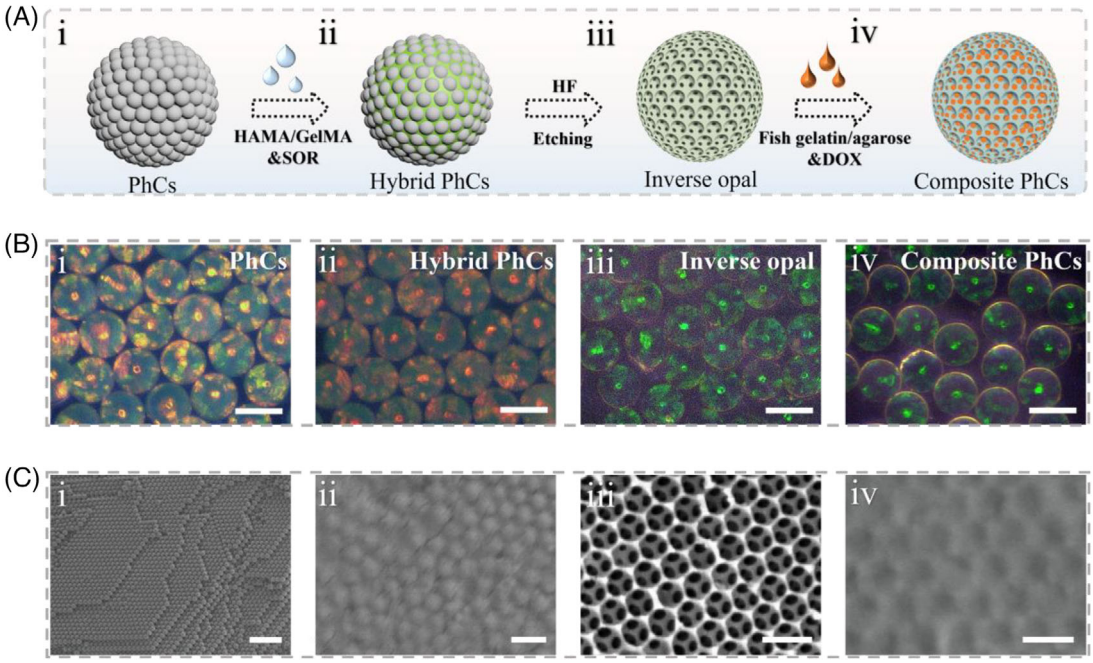

FIGURE 2 (A) Scheme of preparation of different microspheres. (i) photonic crystal template; (ii) hybrid PhCs microsphere; (iii) inverse opal microsphere; (iv) composite microsphere. (B) Microscopic images of different microspheres. (C) SEM images of the structure of corresponding microspheres. Scale bars are all 150 μm in (B) and 1500 nm in (i) of (C) and 500 nm in (ii), (iii), and (iv) of (C).

infiltrated in the nanochannels, which then acted as the main skeleton of the inverse opal after the silica nanoparticles were etched. In addition, owing to the connected porous structure of inverse opal, the secondary filling materials were evenly distributed in the void spaces, thus forming composite microspheres of independent components with the skeleton and filling material (Figure 2C).

In our next experiment, the inverse opal skeleton of the composite microspheres was constructed using hyaluronic acid methacrylate (HAMA) and gelatin methacrylate (GelMA), and the filling hydrogel was fish gelatin and agarose. To endow the composite microspheres with photothermal functions, black phosphorus quantum dots (BPQDs) were incorporated within the filling hydrogel. BPQDs have attracted much interest in the biomedical field because of their effective photothermal capability. Meanwhile, BPQDs possess good biocompatibility and biodegradability, often being used as additives to add into the system. The image of the nanodots and their absorbance spectrum are shown in Figure S1. Using a transmission electron microscope (TEM), it was evident that such BPQDs were in nanoscale with excellent monodispersity (Figure 3A).

The filling hydrogel was composed of a reversible phase-changing hydrogel obtained from a combination of fish gelatin and agarose. The phase transition temperature of fish gelatin/agarose hydrogel with different ratios of agarose was analyzed (Figure S2). The hydrogel composed of 18% fish gelatin and 2% agarose exhibited a melting point at nearly 40.8°C, which is suitable for applying in vivo. Meanwhile, to study the photothermal conversion ability of the composite microspheres with different BPQDs concentrations, near-infrared (NIR) irradiation with different powers including 0.8 W, 1.0 W, 1.2 W, and 1.4 W were applied. As shown in Figure S3, the temperature curve was positively correlated with the concentration of BPQDs and laser intensity. When the concentration of BPQDs was 0.3 mg/mL and the NIR laser intensity was 1.2 W, the temperature change of the microspheres is an ideal profile for photothermal therapy. In this situation, the time-dependent infrared thermal images of the photothermal microspheres with NIR irradiation were recorded in Figure S4. The cyclic heating curve showed outstanding photothermal stability and recyclability of the microspheres (Figure 3B). Besides, as shown in Figure S5, this cyclic heating process did not have a significant effect on the composing material of the inverse opal skeleton (HAMA/GelMA), thus indicating a stable physical structure.

As the composite microspheres possessed different hydrogel components in the skeleton and filling hydrogel, various drugs could be encapsulated in distinct parts to show different release profiles. To observe the distribution of two drugs in the skeleton and the secondary filling material, coumarin (as a model molecule for SOR) and DOX were encapsulated in the inverse opal skeleton and the phase-changing hydrogel, respectively. The microspheres were characterized under a confocal microscope. As exhibited in Figure 3C and Figure S6, the drugs were loaded in the microsphere uniformly. Due to the excellent photothermal conversion efficiency of BPQDs and the adjusted melting point of the secondary filling hydrogel, it underwent a solid-to-liquid phase transition under NIR irradiation, thus promoting the rapid release of wrapped DOX (Figure 3E). In contrast, for coumarin (encapsulated in the skeleton), its difference of release with or without NIR irradiation was relatively less pronounced compared with that of DOX (Figure 3D). Meanwhile, multiple cycles of NIR irradiation were performed to study the photothermal controllable release of DOX. It was obvious that the intervention of NIR greatly promoted the release of drugs in the secondary filling material. Therefore, the drugs showed different release profiles in one system. These results indicated that the proposed composite microsphere system is an ideal spatiotemporal responsive carrier for the on-demand release of multiple drugs.

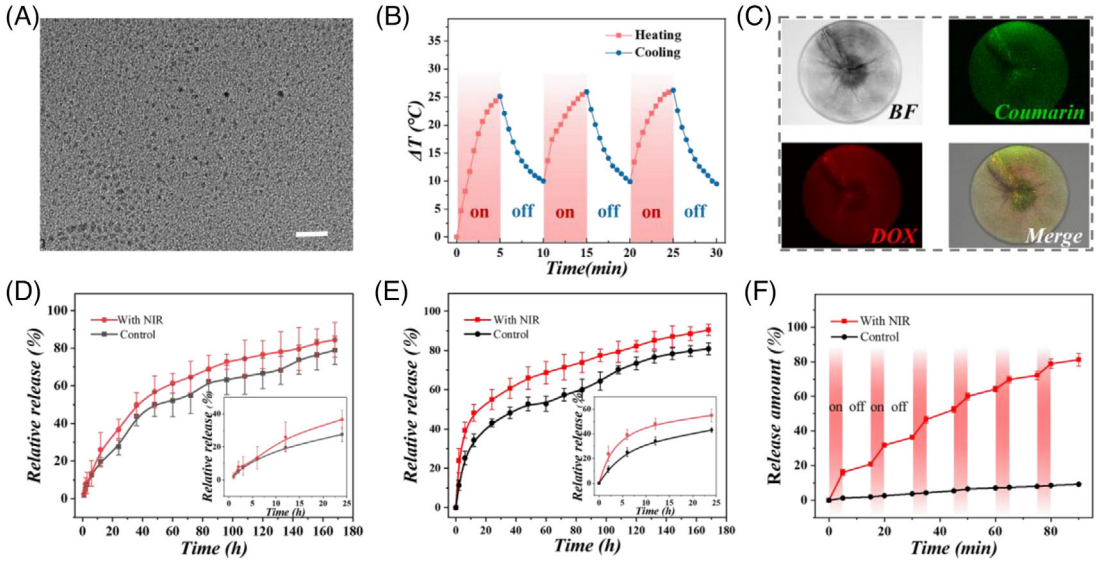

FIGURE 3 (A) TEM image of BPQDs. (B) Cyclic heating curve of the photothermal microspheres. (C) Images of one microsphere loaded with coumarin (in skeleton) and DOX (in phase-changing hydrogel). (D) Release curve of coumarin encapsulated in the inverse opal skeleton for 24 h (inner) and 172 h (outer). (E) Release curve of DOX encapsulated in the secondary filling material for 24 h (inner) and 172 h (outer). NIR irradiation was performed every 12 h. (F) Photocontrolled release of DOX with regular NIR irradiation. Scale bar is 20 nm in (A).

Naturally derived polymer networks typically exhibit excellent biocompatibility. Therefore, hydrogels developed based on such substances have been widely applied in biomedical engineering, including HAMA, GelMA, fish gelatin, and agarose. The biocompatibility of the inverse opal and filling hydrogel was tested, respectively, by co-culture with NIH-3T3 cells. The results showed the similar cell survival rates of these two groups to that in the control group (Figure 4A–D). Moreover, the blood compatibility test of the materials was carried out. The hemolysis rate of both the control group and the experimental group was less than 5%, which showed that the materials possessed excellent blood compatibility (Figure 4E,F). Notably, biodegradability is another important factor for evaluating microcarriers. As shown in Figure S7, the naturally derived hydrogel polymer could lose 80% of its original weight after a week of shaking. These characteristics laid the foundation for the microspheres to act as drug microcarriers.

To confirm the anti-tumor effects of the combined drug delivery system, the SOR and DOX co-loaded composite microspheres were co-cultured with MKN-45 gastric cancer cells, and the fluorescent images of cells were recorded (Figure 4G). Then, the relative cell viability is also shown in Figure S8. The viability of gastric cancer cells did not exhibit an obvious effect in the presence of corresponding materials without drug loading. However, when the drug was loaded, the MKN-45 cell viability decreased significantly, whether in groups treated with mono-drug or multi-drugs. It is worth noting that the group treated with photothermal microspheres plus NIR irradiation showed a certain effect in killing tumor cells. Meanwhile, the use of drug-loaded composite microspheres combined with NIR irradiation rapidly killed tumor cells due to their photothermal effect and fast release of chemotherapeutic DOX.

When applied in the body, it is vital to investigate the location and degradation of foreign material. Hence, the fluorescence-labeled composite microspheres were injected into nude mice. The fluorescent images and degradation curve are shown in Figure S9. To further verify the anti-tumor effect of the spatiotemporal responsive hydrogel microspheres in vivo, we first constructed a tumor-bearing model in nude mice by subcutaneously injecting MKN-45 cells. The intervening treatments were performed after the volume of tumor reached to 100 mm^3. The scheme of animal experiments is shown in Figure 5A. Briefly, the nude mice were allocated into eight groups at random, which received treatments with PBS buffer (G I), drug-free composite microspheres (G II), drug-free photothermal microspheres plus NIR irradiation (G III), microspheres with DOX loading (G IV), microspheres with SOR loading (G V), free DOX and SOR (G VI), microspheres with DOX and SOR loading (G VII), and microspheres with DOX and SOR loading plus NIR irradiation (G VIII). Firstly, we measured the photothermal properties of the composite microspheres in vivo. As shown in Figure 5B, the time-dependent infrared thermal images were recorded, which indicated that the microspheres also maintain excellent photothermal properties even in the body.

The tumor treatment period was 21 days, and the weight changes of the mice were recorded every three days (Figure S10). Tumor samples were cautiously collected after the mice were euthanized (Figure 5C), and their volumes were estimated. As exhibited in Figure 5D,E, the tumors in G I and II grew bigger than those in other groups. Meanwhile, G III treated with composite microspheres plus NIR-induced photothermal therapy also inhibited the growth of tumors to some extent. Compared to that in G VII, G VI showed relatively inferior efficacy, which may be caused by the rapid metabolism of free drugs. In particular, the dual drug-loaded microsphere system possessed a better therapeutic effect than single drug-loaded microspheres, and it showed the best anti-tumor performance when combined with NIR irradiation. This was attributed to the intricate structural features of the composite microspheres, which subtly integrated two drug delivery profiles into one system, enabling on-demand release and synergistic therapy.

To further evaluate the histopathological changes in different groups, H&E staining, TUNEL, and immunofluoresence

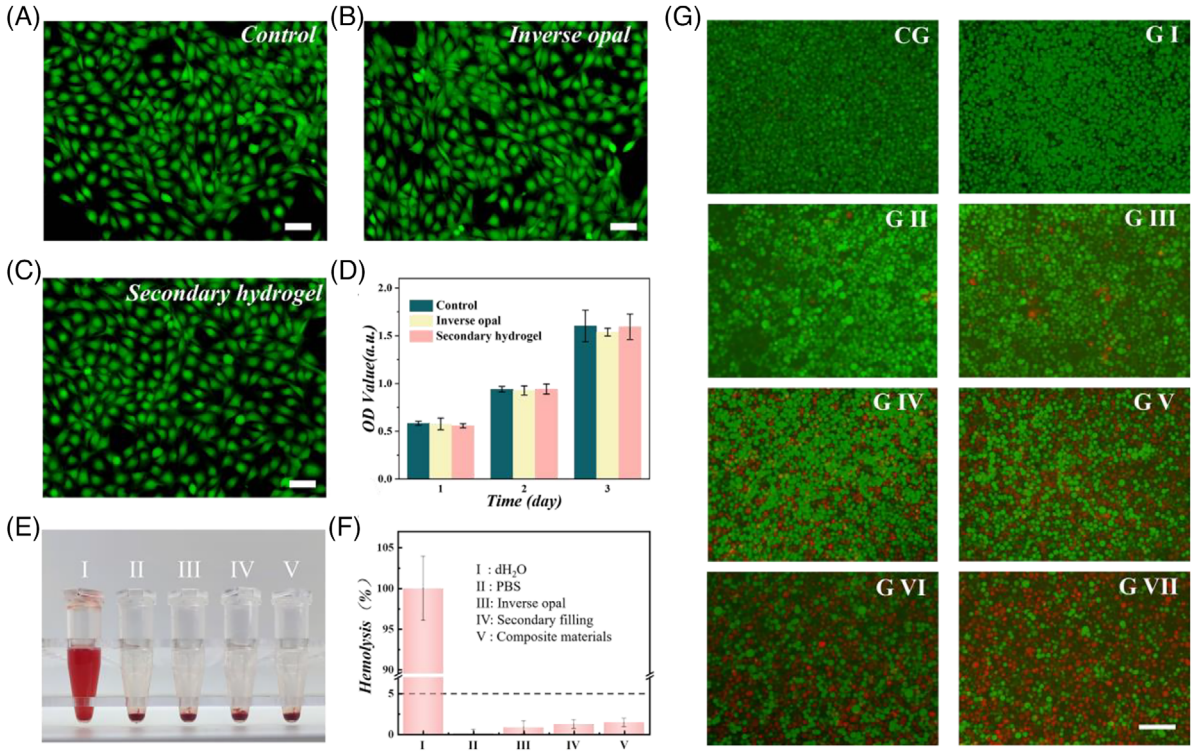

FIGURE 4 (A–C) Fluorescent images of 3T3 cell treated with different materials. The groups are including control, inverse opal, and secondary filling hydrogel, respectively. (D) Statistical analysis of OD value in different groups. (E,F) Images of hemolysis test in groups by different treatments, including deionized water (I), PBS (II), and leaching liquors of inverse opal material (III), secondary filling material (IV), and both inverse opal hydrogel and secondary filling hydrogel (V). (G) Fluorescent images of MKN-45 cells with different treatments, including control (CG), microspheres without drugs (G I), NIR irradiation (G II), drug-free microspheres+NIR (G III), microspheres with SOR encapsulation (G IV), microspheres with DOX encapsulation (G V), microspheres with DOX and SOR encapsulation (G VI), and dual drugs-loaded microspheres+NIR (G VII). Scale bars are 20 μm in (A–C) and (G).

staining were carried out. As shown in Figure 6A, H&E staining images exhibited that the treatment of the spatiotemporal responsive hydrogel microspheres plus NIR irradiation led to obvious apoptosis of tumor cells. In contrast, tumor cells in G I and II demonstrated a higher density and normal volume, with no apparent shrinkage. Besides, the TUNEL staining results indicated a significantly elevated apoptosis rate in G VIII compared to the other groups (Figure 6B and Figure S11a). On the other hand, sorafenib can hinder tumor growth by inhibiting tumor neovascularization and cell proliferation. As exhibited in Figure 6C and Figure S11b, the experimental groups including G V–VIII (supplemented with sorafenib) showed less CD31 expression. Furthermore, no evident pathological damage was found in H&E staining of Group VIII, indicating the ideal in vivo biosafety of the microspheres (Figure S12). All these results indicated that the proposed spatiotemporal responsive microspheres with DOX and SOR loading possessed excellent potential for drug delivery and gastric cancer therapy.

3 | CONCLUSION

In summary, we have proposed a drug-delivery system based on IOMPs with desirable spatiotemporal responsiveness for gastric cancer therapy. The IOMPs-based composite microspheres were composed of HAMA and GelMA skeleton, with a secondary hydrogel filling hydrogel consisting of fish gelatin and agarose. The microspheres integrated two drug release modes including NIR-induced rapid release of DOX as well as sustained release of SOR, thus realizing the spatiotemporal responsive on-demand release of different drugs in a single system. Given these properties, it was demonstrated that the microspheres possessed the desired properties of the on-demand release of drugs and enhanced the efficiency of tumor therapy. These results indicated that the present spatiotemporal responsive hydrogel microspheres owned valuable application potentials for drug delivery and tumor therapy.

4 | EXPERIMENTAL SECTION

4.1 | Materials and animals

Doxorubicin (DOX), sorafenib (SOR), methacrylic anhydride (MA), gelatin, fish gelatin, agarose, coumarin, and chitosan were purchased from Sigma-Aldrich (St. Louis, MO, USA). Hydrofluoric acid and n-hexadecane were brought from Aladdin Industrial Corporation. HAMA and GelMA were manufactured according to previous work. CCK-8 Assay Kit purchased from Beyotime Biotechnology. Black Phosphorus quantum dots were purchased from Xianfeng Nano Technology Co., Ltd. Water obtained from a purification system (Milli-Q).

4.2 | Construction of photonic crystal (PhCs) template

The droplet microfluidic technology was employed to construct PhCs templates. The concentration of the silica

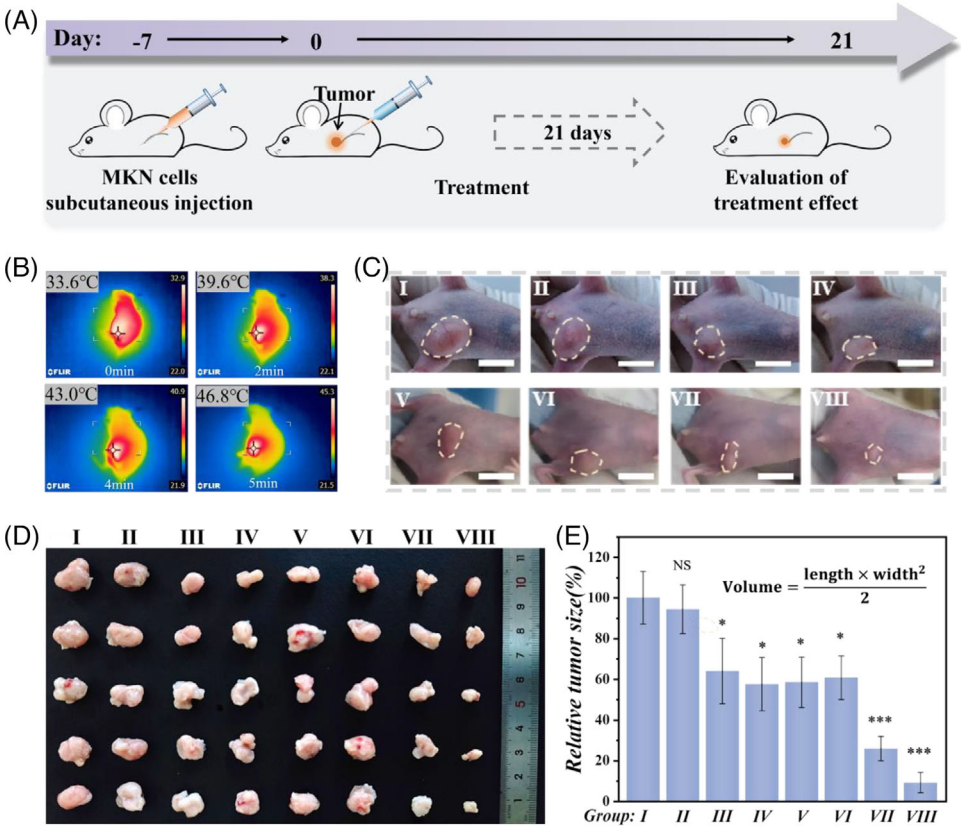

FIGURE 5 (A) Flowchart of the use of the composite microspheres for tumor therapy. (B) Infrared thermal images of mice under NIR irradiation after intratumor injection of photothermal microspheres. (C) Photographs of the mice in different groups and their tumor size as indicated. (D) Photographs of tumors in each group at day 21. (E) Estimated relative tumor size of mice suffered from different treatments at day 21. Groups: PBS buffer (G I), composite microspheres without drugs (G II), photothermal microspheres with NIR irradiation (G III), microspheres loaded with DOX (G IV), microspheres loaded with SOR (G V), free DOX and SOR (G VI), microspheres loaded with DOX and SOR (G VII), and microspheres loaded with DOX and SOR plus NIR irradiation (G VIII). Scale bars are 1 cm in (C).

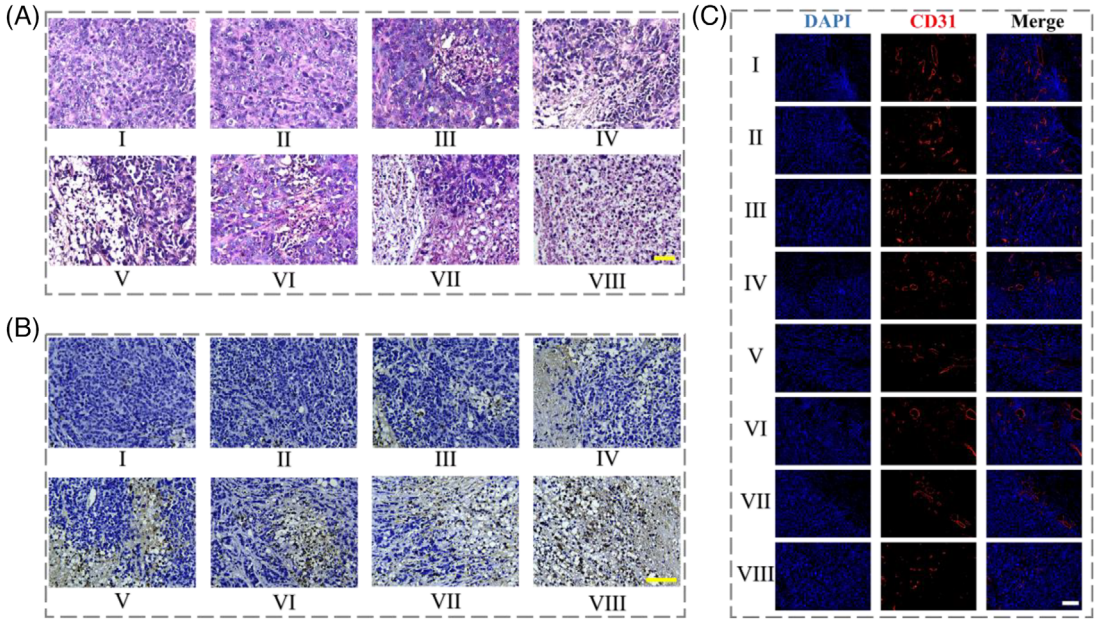

FIGURE 6 (A) H&E stained tumor sample images from each group. (B) TUNEL staining of tumor samples from each group. (C) Fluorescence images of CD31 impression in tumor. Groups: PBS buffer (G I), composite microspheres without drugs (G II), photothermal microspheres with NIR irradiation (G III), microspheres loaded with DOX (G IV), microspheres loaded with SOR (G V), free DOX and SOR (G VI), microspheres loaded with DOX and SOR (G VII), and microspheres loaded with DOX and SOR plus NIR irradiation (G VIII). Scale bars are 100 μm in all.

nanoparticles solution was initially adjusted to approximately 20% (w/v). Subsequently, in the production of emulsion droplets, the silica aqueous solution was used as the internal phase, and n-hexadecane containing 1% surfactant 2296 served as the external phase, both flowing in a microfluidic device. Water-in-oil droplets were produced in the device, which were then collected in a collection bath. The droplets were then subjected to 75°C for 10 h on a hot table, allowing for the self-assembly of the nanoparticles through water evaporation. Last, the PhCs microspheres were calcined at 800°C for 6 h to enhance their mechanical strength.

4.3 | Preparation of porous inverse opal microparticles (IOMPs)

A pregel solution was prepared, primarily consisting of 0.1 g/mL HAMA, 0.04 g/mL GelMA, and 1% photoinitiator HMPP. Subsequently, the as-prepared PhCs template particles were immersed with the pregel solution for approximately 30 min, by which the capillary force facilitated infiltration of the pregel into the nanoholes of the silica nanoparticles. Polymerization of the pregel was then carried out using UV light, by which the hybrid particles were stripped from the gel. Such hybrid microparticles were subjected to immersion in 4% hydrofluoric acid to remove the silica nanoparticles. The IOMPs obtained were then washed and cleaned for further use.

4.4 | Regulation of melting point of secondary filling hydrogel

The secondary filling material with different ratios of agarose was measured to find the appropriate melting temperature. Specifically, the total concentration of the two components was kept at 20%; the concentration of agarose ranged from 0% to 3.5%, with increments of 0.5%.

4.5 | Preparation of photothermal composite microspheres

Based on the IOMPs, we mixed the IOMPs with the secondary filling material doped with BPQDs and made the secondary filling material fully fill the hole of IOMPs under the conditions of centrifugation or vacuum negative pressure. To optimize the photothermal performance, we also studied the effect of BPQDs concentration and near-infrared (NIR) light power on the temperature rise of the microspheres. SEM was used to characterize the four types of microspheres. It is worth noting that because the hydrogel is prone to collapse during the sample preparation process, resin was used here for shooting.

4.6 | Drug encapsulation and release experiment in vitro

For drug encapsulation, the pregel of IOMP polymer was doped with SOR for its encapsulation in the skeleton. Then, DOX was wrapped into the phase-changing hydrogel to fill the voids of the IOMPs under negative pressure. The blended composition underwent cooling and re-solidification. Subsequently, the resultant solid subject was immersed in a buffer solution. Following this immersion, the dislodged drug-loaded particles were gathered after a delicate crushing process. To study this drug release behavior of the microspheres, the fluorescence intensity of the microspheres was measured. Coumarin was used as a substitute for SOR. The microspheres underwent incubation in 1 mL of phosphate-buffered saline (PBS) with gentle agitation at ambient temperature. Collagenase was also added to the solution. Subsequently, 100 μL of the buffer solution was extracted from a 96-well plate at hourly intervals for fluorescence intensity measurement. Meanwhile, an equal amount of PBS was added back into the system. For short-term release experiments, the group treated with drug-loaded microparticles, followed by NIR irradiation using a laser (808 nm, 1.2 W, 10 cm) for a duration of 5 min, underwent subsequent cooling for a period of 10 min. The sampling procedure is the same as above. For that in the long-term release profile, NIR irradiation was performed on a daily basis.

4.7 | Biocompatibility experiment

To assess the biocompatibility of materials, a CCK-8 test was performed. In this section, we set up a control group and two experimental groups, each group comprising three parallel samples. Cells in the control group were solely treated with a culture medium, those in experimental group I were cultured with IMOPs, and those in experimental group II were treated with a hydrogel consisting of fish gelatin and agarose. NIH 3T3 cells were seeded in a 24-well plate and co-incubated with the respective groups for 24, 48, and 72 h in an incubator. After that, a portion of the culture medium was removed, and CCK-8 reagent was added at a final concentration of 10%. The reaction was maintained for 2–4 h, and cellular viability was assessed through the quantification of OD value employing a microplate reader. Additionally, the cell viability was assessed each day using cell fluorescent staining for all experimental groups.

4.8 | In vitro antitumor effects

MKN-45 cells were seeded in a 24-well plate, each well seeded with 5×10^4 cells. The cells were allowed to attach for one night. Then, different treatments were administered to the MKN-45 cells, including a control group (CG), microparticles without drugs (G I), NIR irradiation (G II), photothermal microspheres combined with NIR (G III), microspheres encapsulated with SOR (G IV), microspheres encapsulated with DOX (G V), microspheres encapsulated with both DOX and SOR (G VI), and dual drug-loaded microspheres combined with NIR (G VII). The dosage of DOX and SOR were set as 3 μg/mL and 4 μg/mL, respectively. The group treated with NIR irradiation was irradiated with a laser (808 nm, 1.2 W, 10 cm) for 5 min. Subsequently, live/dead staining and CCK8 assay were performed. Cell viability was assessed through live/dead staining, which included the application of Calcein-AM and propidium iodide (PI) to the cells. Subsequently, the stained cells were examined using a fluorescence

microscope. In the CCK-8 test, cells were added with the CCK-8 reagent for a duration of 2–4 h, and the absorbance was quantified employing a microplate reader.

4.9 | In vivo anti-tumor evaluation

Animal experiments were approved by Ethical Committee of Wenzhou Institute, University of Chinese Academy of Sciences (WIUCAS22062103). For the in vivo fluorescence and degradation test, the fluorescence-labeled microspheres were injected into nude mice. The fluorescence images were shot every three days. For the in vivo anti-tumor test, subcutaneous injection of 1×10^6 MKN-45 cells was performed under the leg of nude mice. Then, tumor growth was allowed until the volume reached approximately 100 mm^3 to ensure the smallest difference in tumor volume. Next, the mice were randomly assigned into eight groups ($n = 5$) as follows: PBS buffer (G I), composite microspheres without drugs (G II), photothermal microspheres with NIR irradiation (G III), microspheres loaded with DOX (G IV), microspheres loaded with SOR (G V), free DOX and SOR (G VI), microspheres loaded with DOX and SOR (G VII), and microspheres loaded with DOX and SOR plus NIR irradiation (G VIII). The dosage of DOX and SOR were set as 15 mg/kg and 20 mg/kg, respectively. The body weights were recorded every three days, and euthanasia was performed after 21 days. The principal organs and tumors were harvested and preserved in 4% (v/v) paraformaldehyde. Tumor samples were embedded and sliced for subsequent staining procedures, including H&E staining and terminal-deoxynucleotidyl transferase-mediated nick end labeling (TUNEL) staining. Furthermore, immunofluorescence staining for CD31 was performed to evaluate the vascular distribution within the tumor tissues.

4.10 | Statistical analysis

The results were presented as mean values accompanied by standard deviations (SD). To assess the significance of the findings, statistical analysis was conducted using either the Student's *t*-test or one-way ANOVA, followed by Tukey's post-hoc test, as appropriate. Significance levels were denoted as follows: NS (not significant), $*p < 0.05$, $**p < 0.01$, $***p < 0.001$.

AUTHOR CONTRIBUTIONS

Li Wang: Methodology; data curation; writing—original draft preparation. **Lu Fan**: Supervision; writing—reviewing and editing. **Anne M. Filppula**: Writing—reviewing and editing. **Yu Wang:** Conceptualization; writing—reviewing and editing. **Luoran Shang**: Conceptualization; supervision; writing—reviewing and editing. **Hongbo Zhang**: Funding acquisition; supervision; writing—reviewing and editing.

ACKNOWLEDGMENTS

The authors appreciate the financial support from the National Natural Science Foundation of China (82372145), the Research Fellow (Grant No. 353146), Research Project (347897), Solutions for Health Profile (336355), InFLAMES Flagship (337531) grants from Academy of Finland, and the Finland China Food and Health International Pilot Project funded by the Finnish Ministry of Education and Culture.

CONFLICT OF INTEREST STATEMENT

The authors declare no conflicts of interest.

DATA AVAILABILITY STATEMENT

The data that support the findings of this study are available from the corresponding author upon reasonable request.

ORCID

Li Wang https://orcid.org/0000-0001-5543-3725
Luoran Shang https://orcid.org/0000-0001-7458-9100
Hongbo Zhang https://orcid.org/0000-0002-1071-4416

REFERENCES

1. S. Cornen, E. Vivier, *Science* **2018**, *362*, 1355.
2. M. Xu, T. Zhang, R. Xia, Y. Wei, X. Wei, *Mol. Cancer* **2022**, *21*, 208.
3. Q. Lei, S.-B. Wang, J.-J. Hu, Y.-X. Lin, C.-H. Zhu, L. Rong, X.-Z. Zhang, *ACS Nano* **2017**, *11*, 7201.
4. J. Yang, H. Yao, Y. Guo, B. Yang, J. Shi, *Angew. Chem. Int. Ed.* **2022**, *61*, e202200480.
5. L. Huang, S. Zhao, J. Wu, L. Yu, N. Singh, K. Yang, M. Lan, P. Wang, J. S. Kim, *Coord. Chem. Rev.* **2021**, *438*, 213888.
6. M. Zhang, R. Song, Y. Liu, Z. Yi, X. Meng, J. Zhang, Z. Tang, Z. Yao, Y. Liu, X. Liu, W. Bu, *Chem* **2019**, *5*, 2171.
7. Y. Wang, X. Ma, W. Zhou, C. Liu, H. Zhang, *Smart Med.* **2022**, *1*, e20220013.
8. H. Zou, S. Gan, H. Shen, B. He, Z. Zheng, J. Li, J. C. Huang, L. Zheng, B. Z. Tang, J. Zhang, *Mater. Today* **2022**, *61*, 117.
9. M. Michael, M. M. Doherty, *J. Clin. Oncol.* **2016**, *23*, 205.
10. S. Li, Y. Zhang, S.-H. Ho, B. Li, M. Wang, X. Deng, N. Yang, G. Liu, Z. Lu, J. Xu, Q. Shi, J.-Y. Han, L. Zhang, Y. Wu, Y. Zhao, G. Nie, *Nat. Biomed. Eng.* **2020**, *4*, 732.
11. D. Tang, Y. Yu, J. Zhang, X. Dong, C. Liu, H. Xiao, *Adv. Mater.* **2022**, *34*, 2203820.
12. V. Sridhar, F. Podjaski, Y. Alapan, J. Kröger, L. Grunenberg, V. Kishore, B. V. Lotsch, M. Sitti, *Sci. Rob.* **2022**, *7*, eabm1421.
13. H. M. Kim, S. A. Kim, S. B. Park, J. H. Cho, S. Y. Song, *Scand. J. Gastroenterol.* **2017**, *52*, 577.
14. H. Zou, Z. Wei, C. Song, J. Ran, Z. Cao, C. Tang, G. Zhang, Y. Cai, M. Lu, W. Han, *J. Mater. Chem. B* **2021**, *9*, 3235.
15. J. Wan, J. Wang, M. Zhou, Z. Rao, X. Ling, *J. Mater. Chem. B* **2020**, *8*, 7755.
16. W. Chen, K. Shi, J. Liu, P. Yang, R. Han, M. Pan, L. Yuan, C. Fang, Y. Yu, Z. Qian, *Bioact. Mater.* **2023**, *23*, 1.
17. S.-Y. Qin, Y.-J. Cheng, Q. Lei, A.-Q. Zhang, X.-Z. Zhang, *Biomaterials* **2018**, *171*, 178.
18. Q. Song, C. Zheng, J. Jia, H. Zhao, Q. Feng, H. Zhang, L. Wang, Z. Zhang, Y. Zhang, *Adv. Mater.* **2019**, *31*, 1903793.
19. J. Kaiser, *Science* **2020**, *369*, 18.
20. D. Liang, G. Kuang, X. Chen, J. Lu, L. Shang, W. Sun, *Smart Med.* **2023**, *2*, e20230016.
21. X. Su, Z. Bao, W. Xie, D. Wang, T. Han, D. Wang, B.Z. Tang, *Research* **2023**, *6*, 0194.
22. W. Zhou, X. Ma, J. Wang, X. Xu, O. Koivisto, J. Feng, T. Viitala, H. Zhang, *Smart Med.* **2022**, *1*, e20220036.
23. C. Gong, X. Zhang, M. Shi, F. Li, S. Wang, Y. Wang, Y. Wang, W. Wei, G. Ma, *Adv. Sci.* **2021**, *8*, 2002787.
24. L. Wang, Z. Cao, M. Zhang, S. Lin, J. Liu, *Adv. Mater.* **2022**, *34*, 2106669.
25. Y. Chen, M. Du, Z. Yuan, Z. Chen, F. Yan, *Nat. Commun.* **2022**, *13*, 4468.
26. H. Zhang, Y. Liu, G. Chen, H. Wang, C. Chen, M. Li, P. Lu, Y. Zhao, *Sci. Bull.* **2020**, *65*, 380.
27. Y. S. Zhang, C. Zhu, Y. Xia, *Adv. Mater.* **2017**, *29*, 1701115.
28. H. Lee, T. Y. Jeon, S. Y. Lee, S. Y. Lee, S.-H. Kim, *Adv. Funct. Mater.* **2018**, *28*, 1706664.

29. F. Bian, L. Sun, H. Chen, Y. Wang, L. Wang, L. Shang, Y. Zhao, *Adv. Sci.* **2022**, *9*, 2105278.
30. X. Shou, H. Zhang, D. Wu, L. Zhong, D. Ni, T. Kong, Y. Zhao, Y. Zhao, *Small* **2021**, *17*, 2006955.
31. C. Chen, Y. Liu, H. Wang, G. Chen, X. Wu, J. Ren, H. Zhang, Y. Zhao, *ACS Nano* **2018**, *12*, 10493.
32. X. Shou, Y. Liu, D. Wu, H. Zhang, Y. Zhao, W. Sun, X. Shen, *Chem. Eng. J.* **2021**, *408*, 127349.
33. L. Wang, L. Sun, F. Bian, Y. Wang, Y. Zhao, *ACS Nano* **2022**, *16*, 2640.
34. H. Wang, X. Chen, G. Xie, D. Bi, S. Du, M. Li, L. Zhang, J. Zhu, *Adv. Funct. Mater.* **2023**, *33*, 2306025.

SUPPORTING INFORMATION

Additional supporting information can be found online in the Supporting Information section at the end of this article.

How to cite this article: L. Wang, L. Fan, A. M. Filppula, Y. Wang, L. Shang, H. Zhang, *Aggregate* **2024**, e600. https://doi.org/10.1002/agt2.600